

Supporting Information

Bio-Inspired Electrode Design: Bulk Iron-Nickel Sulfide Allows for Efficient Solvent-Dependent CO₂ Reduction

Stefan Piontek,^a Kai junge Puring,^{a,b} Daniel Siegmund,^b Mathias Smialkowski,^a Ilya Sinev,^c David Tetzlaff,^a

*Beatriz Roldan Cuenya,^d and Ulf-Peter Apfel^{*a,b}*

[a] S. Piontek, K. junge Puring, M. Smialkowski, D. Tetzlaff, Dr. U.-P. Apfel, Inorganic Chemistry I, Ruhr-Universität Bochum, Universitätsstrasse 150, 44780 Bochum (Germany)

[b] K. junge Puring, Dr. D. Siegmund, Dr. U.-P. Apfel, Fraunhofer UMSICHT, Osterfelder Straße 3, 46047 Oberhausen (Germany)

[c] Dr. I. Sinev, Department of Physics, Ruhr-University Bochum, Universitätsstrasse 150, 44780 Bochum (Germany)

[d] Prof. Dr. B. Roldan Cuenya, Department of Interface Science, Fritz-Haber Institute of the Max Planck Society, Faradayweg 4-6, 14195 Berlin (Germany)

Author Information

Corresponding Author

*E-mail: ulf.apfel@rub.de

ORCID

Ulf-Peter Apfel: 0000-0002-1577-2420

Beatriz Roldan Cuenya: 0000-0002-8025-307X

Daniel Siegmund: 0000-0003-2476-8965

Ilya Sinev: 0000-0002-0230-0299

Materials. All chemicals were obtained from commercial vendors and used without further purification. High-purity iron, nickel and sulfur powders were obtained from Sigma Aldrich. Acetonitrile was dried using an MBraun Solvent Purification System.

Preparation of Fe_{4.5}Ni_{4.5}S₈. The high temperature synthesis of pentlandite (Fe_{4.5}Ni_{4.5}S₈) and electrode preparation was performed following published procedures.^[1]

Electrochemical Experiments. Electrochemical experiments were performed in a two-compartment H-type cell with a total volume of 215 ml. The half-cells were separated by a cation exchange membrane (CEM, fumasep F-10100). During the experiments, the H-type cell was continuously purged with CO₂ (≥ 99.9Vol.%, Air Liquide) at a constant rate of 20 ml min⁻¹. A blank run was performed in the presence of argon gas (≥ 99.999 %, Air Liquide) and revealed CO₂ as the sole source of all observed CO₂RR products. All experiments were performed using 0.1 M TBAPF₆ (tetrabutylammonium hexafluorophosphate) as an electrolyte in the respective solvent. Electrochemical measurements were performed using a GAMRY Reference 600 or 600+ potentiostat with a three-electrode setup. The self-made working (as prepared Fe_{4.5}Ni_{4.5}S₈)^[1] and the reference electrode (Ag|AgCl (sat. KCl)) were mounted to the same half-cell, separated from the counter electrode (Pt-grid) by the CEM. Linear sweep experiments were performed in a potential range of -0.0V to -2.2 V vs NHE with a sweep rate of 5 mV s⁻¹. Long-term stability measurements were performed via controlled potential coulometry (CPC) at a constant potential of -1.8 V vs NHE for all experiments if not otherwise stated. The overall cell potential applied between the working and counter electrode was separately measured in dry acetonitrile with a voltmeter and was determined as 3.2, 4 and 4.8 V at a set potential between the reference and working electrode of -1.2, -1.5 and -1.8 V vs NHE respectively. Therefore, the applied potential at the counter electrode/anode is always below 3 V and renders the oxidative decomposition of the solvent under the herein applied conditions unlikely.^[29]

Quantification of the reduction products. Quantification of the headspace gas composition within the H-type cell was performed using an Agilent Technologies 7820A gas chromatograph equipped with a thermal conductivity (TCD) and a flame ionization detector (FID) as well as a methanizer. Gas separation was performed using a two-column separation system (HP-PLOT Q 30 m x 0.53 mm x 40 μm column & HP-Molesieve 5 Å 30 m x 0.53 mm x 25 μm) using argon as the carrier gas.

Analyses of the solubilized electrocatalytic products was performed via high pressure liquid chromatography (HPLC) after 10 hours of electrolysis using a Kontron Instruments 465 autosampler equipped with a UV/vis 430A detector. A 250/4 Nucleodur C18 Pyramid, 5 μm (Macherey Nagel) using a linear gradient of 50 mM KH₂PO₄/ H₃PO₄ (0.14

M) (pH 1.5) was used for the quantification of organic acids. Quantification of alcohols was performed using an Agilent Technologies 7890B gas chromatograph equipped with a DB-VRX column and a FID. The exact water concentration of the organic solvents was determined by coulometric titration via Karl Fischer titrator using a TitroLine 7500 KF trace.

Isotope labeling studies. The isotope labeling studies were performed under the conditions as stated under quantification of the reduction products. The mass selective analyses were performed with a GC-MS QP2020 (Shimadzu) utilizing a HP-Plot/Q column in the presence of ^{13}C O (Sigma Aldrich) or CD_3CN (Eurisotope).

Table S1. Water concentration as determined by Karl-Fischer titration and pka values in the different solvents.

Solvent	Water content	pK_a
MeOH	500 ppm	16
MeCN	113 ppm	25
DMSO	170 ppm	35
DMF	1500 ppm	-0.65
Pyridine	160 ppm	5.2
Formic acid	37%	3.8
Oxalic acid	0.1 M	1.2/4.2
Acetic acid	0.1 M	4.8

Table S2. Water concentration in acetonitrile determined by Karl-Fischer titration.

Solvent	Karl-Fischer Titration*
MeCN 24	23.3
MeCN113	110.5
MeCN 500	649.7
MeCN 5000	4612.0
MeCN 30000	Added manually

* + 0.1M TBAPF₆

Table S3. Adjustable CO to H₂ ratios upon CO₂ reduction in acetonitrile at different water concentrations and applied potentials.

Potential (V vs NHE)	-1.2	-1.5	-1.8
Water Content	Ratio	Ratio	Ratio
24 ppm	7 : 1	11 : 1	1 : 27
113 ppm	3 : 1	12 : 1	1 : 12
500 ppm	14 : 1	11 : 1	1 : 3
5000 ppm	24 : 1	24 : 1	3 : 1
30000 ppm	43 : 1	29 : 1	8 : 1

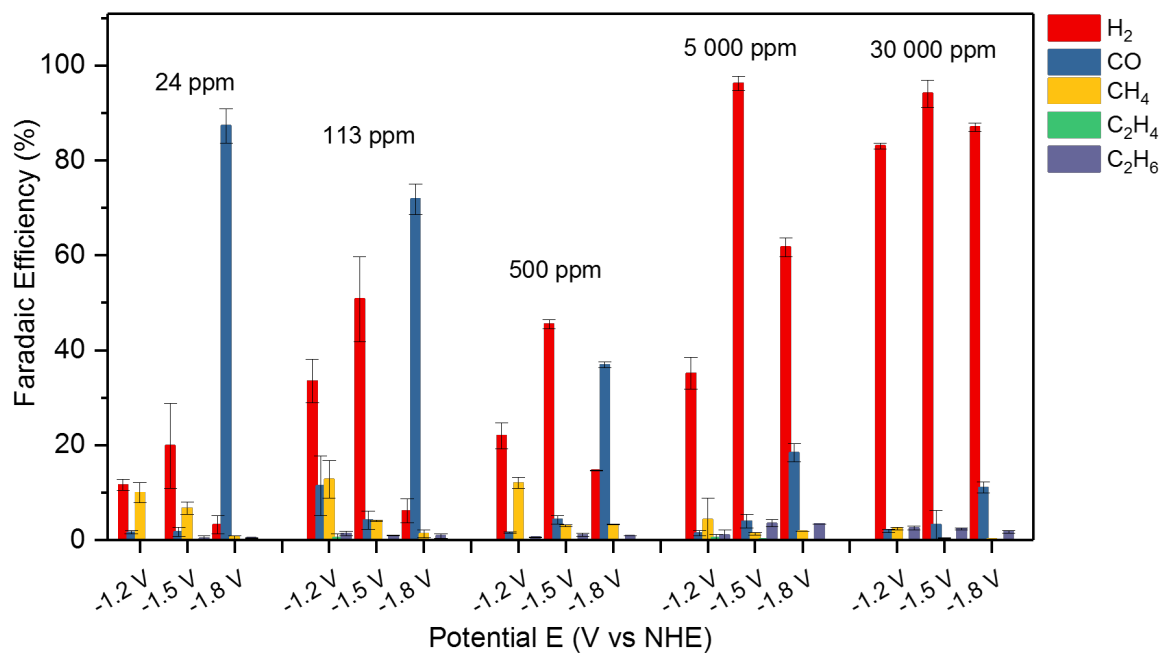


Figure S1. Overview of the product distribution upon CPC CO₂ reduction experiments with variable water concentrations. The experiments were performed independently 3 times using a fresh Fe_{4.5}Ni_{4.5}S₈ electrode.

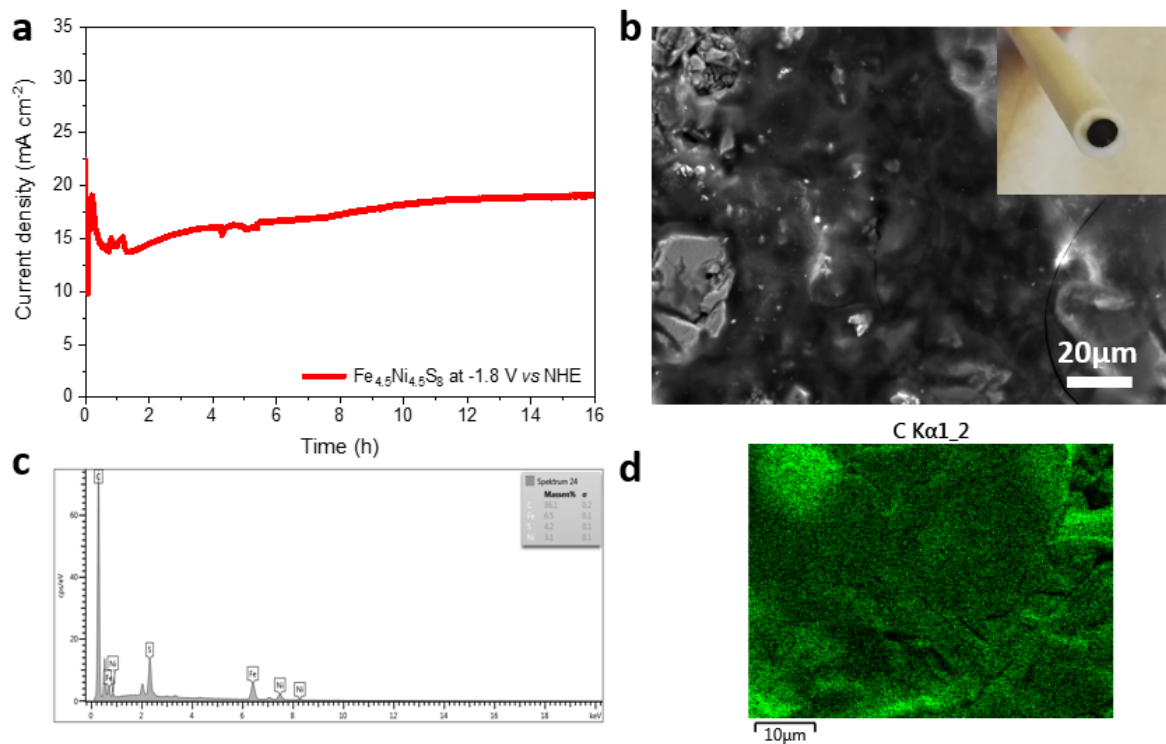


Figure S2. Stability test in acetonitrile with a water concentration of 5000 ppm at an applied potential of -1.8 V vs NHE for the CO_2RR (a), SEM image of the electrode surface (b), EDX analysis reveals a high carbon content (c) and EDS image of carbon (d).

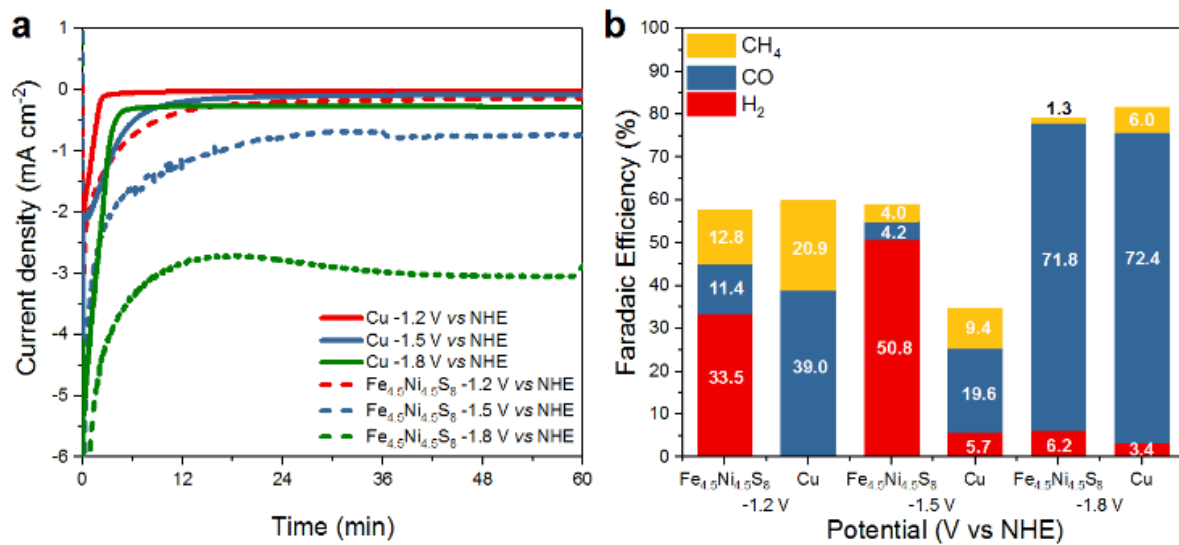


Figure S3. Potential-dependent CPC of Fe_{4.5}Ni_{4.5}S₈ and Cu in MeCN with a water concentration of 113 ppm from -1.2 V to -1.8 V vs NHE (a) and quantification of gas products for both compounds (b).

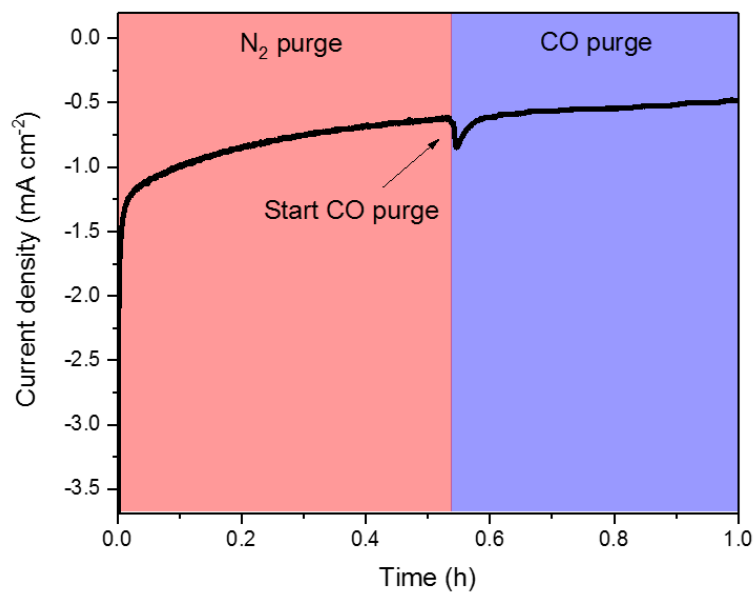


Figure S4. CO poisoning experiment in MeCN containing 24 ppm water using bulk $\text{Fe}_{4.5}\text{Ni}_{4.5}\text{S}_8$. The solution was purged with N_2 while applying a constant potential of -1.8 V vs NHE. Subsequently, CO was purged through the solution revealing no change in catalytic current.

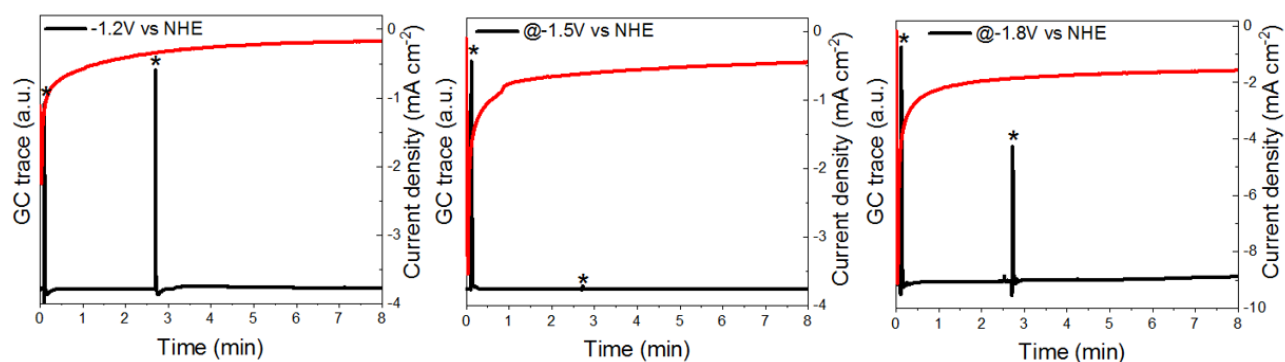


Figure S5. Quantification of gaseous CO₂ reduction products via gas chromatography after 1 hour of CPC experiments while continuously purging with CO. No CO conversion was observed after 1 hour of electrolysis. The indicated (*) signal shows the valve shifts of the GC.

Table S4. Overview of non-noble catalysts for the CO₂ reduction reaction.

Catalyst	Electrolyte	Conditions	Products (FE %)*	Ref.
Bulk Cu	0.1 M KHCO ₃	-0.99 V vs RHE	CH ₄ (1.5), C ₂ H ₄ (27.2)	[2]
Plasma-activated Cu-nanocube	0.1 M KHCO ₃	-1.0 V vs RHE	CO (0.5), C ₂ H ₄ (45)	[3]
Plasma-oxidized Cu foil	0.1 M KHCO ₃ + 0.3 M KI	-1.0 V vs RHE	C ₂ H ₄ (48)	[4]
Cu ₂ O-derived Cu films	0.1 M KHCO ₃	-0.98 V vs RHE	CH ₄ (2), C ₂ H ₄ (31)	[5]
Bi-Phasic Cu ₂ O-Cu	0.1 M KCl	-1.6 V vs RHE	CH ₄ (1.4), C ₂ H ₄ (22), C ₂ H ₆ (1), C ₃ H ₆ (0.9), C ₃ H ₈ (1), C ₄ H ₁₀ (0.9)	[6]
Oxide-derived Cu foam	0.5 M NaHCO ₃	-0.7 V vs RHE	CO (25), C ₂ H ₄ (15), C ₂ H ₆ (37)	[7]

Cu-halide confined mesh	3 M KBr	-2.4 V vs Ag AgCl	CO (2.4), CH ₄ (5.8), C ₂ H ₄ (79.5), C ₂ H ₆ (1.2),	[8]
Oxide-derived Cu	0.1 M CsHCO ₃	-1.0 V vs RHE	CO (<3), CH ₄ (0.93), C ₂ H ₄ (45)	[9]
Bulk Ag	[BMIM]Cl/H ₂ O	-1.5 V vs SCE	CO (99)	[10]
Bulk Ag	0.1 M KHCO ₃	-1.4 V vs NHE	CO (82)	[11]
Bulk Fe	30 atm, KHCO ₃	-1.63 V vs Ag AgCl	CO (4), CH ₄ (2), C ₂ H ₄ (0.24), C ₂ H ₆ (0.4)	[12]
Bulk In	0.1 M TEAP/PC	-2.6 V vs Ag AgCl	CO (85)	[13]
Bulk Zn	0.1 M TEAP/ H ₂ O	-2.0 V vs SCE	CO (36)	[13]
Bi/GC	EMIM-BF ₄ /MeCN	-1.95 V vs SCE	CO (95)	[14]
Bi/GC	[BMIM]PF ₆ /MeCN	-1.80 V vs SCE	CO (85)	[15]
FeN _x /C	0.1 M Na ₂ SO ₄	-0.6 V vs RHE	CO (90)	[16]
Ni-N	1 M KHCO ₃	-1.03 V vs RHE	CO (98)	[17]
CoPc-CNT	0.1 M KHCO ₃	-0.63 V vs RHE	CO (98)	[18]
Ni ₅ Ga ₃	0.1 M KHCO ₃	-0.88 V vs RHE	CH ₄ (2.1), C ₂ H ₄ (0.4), C ₂ H ₆ (1.7)	[19]
MoS ₂	EMIM-BF ₄ /H ₂ O (4:96)	-0.8 V vs RHE	CO (98)	[20]
WSe ₂	EMIM-BF ₄ /H ₂ O (1:1)	-0.8 V vs RHE	CO (92)	[21]
Mo ₂ C	0.1 M KHCO ₃	-0.50 V vs RHE	CH ₄ (1.6)	[22]
RE-Zn	0.5 M KCl	-0.95 V vs RHE	CO (95)	[23]

* Faradaic efficiencies are exclusively reported for gaseous products.

Table S5. Table of different CO₂ solubilities in the utilized organic solvents.

Solvent	Mole fraction	CO ₂ Solubility	Ref.
H ₂ O	0.0007	0.04 M	[24]
MeOH	0.0063	0.16 M	[25]
MeCN	0.0141	0.27 M	[26]
DMSO	0.0018	0.02 M	[27]
DMF	0.0142	0.18 M	[25]
Pyridine	0.0118	0.15 M	[25]
Propylene carbonate	0.5880	6.97 M	[28]

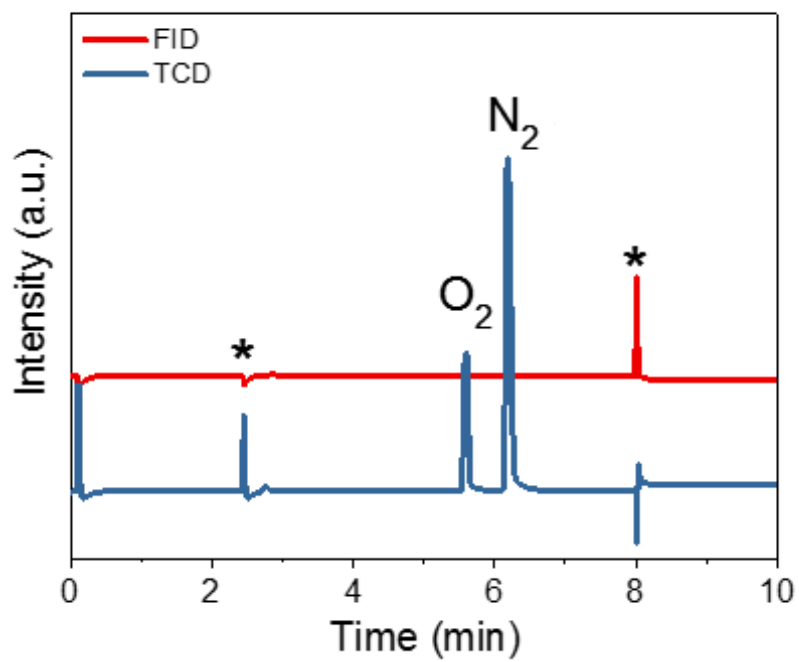


Figure S6. Argon measurements after 1 h CPC using a $\text{Fe}_{4.5}\text{Ni}_{4.5}\text{S}_8$ electrode at -1.8 V in MeCN with 24 ppm water concentration showing no formation of C_1 - C_2 products. The indicated (*) signal shows the valve shifts of the GC.

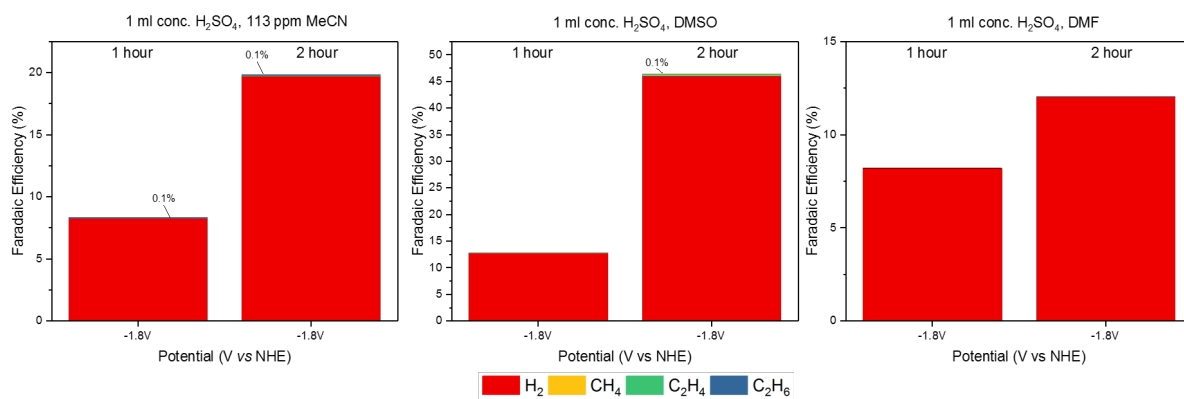


Figure S7. Quantification of gaseous products in the absence of CO₂ after 1 and 2 hours of CPC respectively using a fresh Fe_{4.5}Ni_{4.5}S₈ electrode. Sulfuric acid was added to compensate for low current densities in these otherwise noncatalytic conditions.

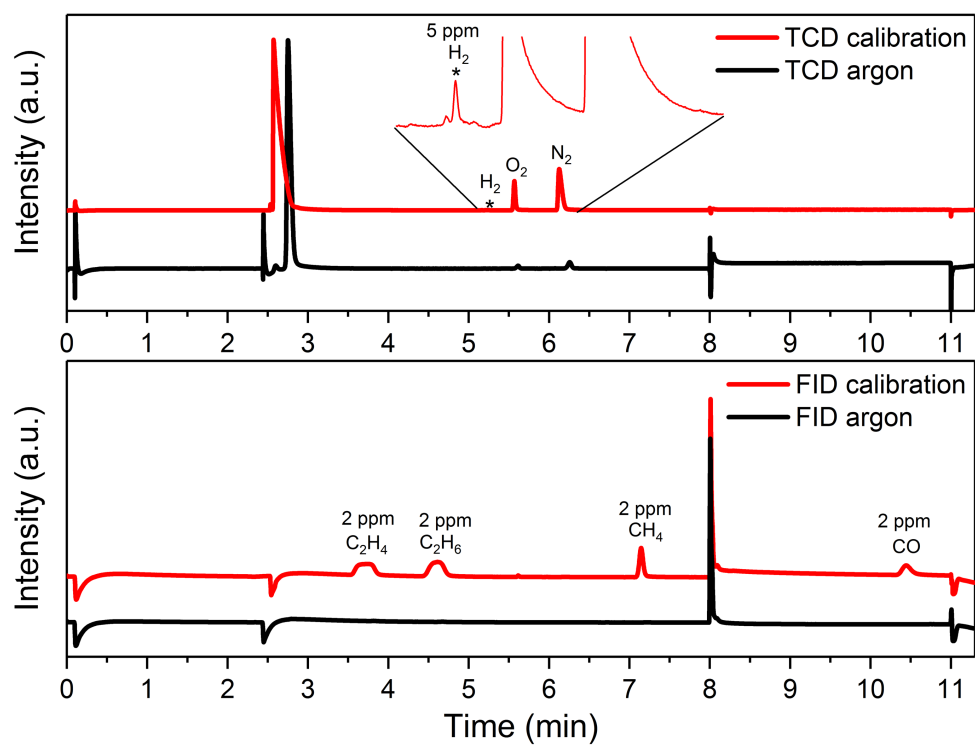


Figure S8. GC control experiments using commercial calibration gas with defined fractions of H₂, C₁-C₂ products and blank measurements with argon. The GC traces are shown for the thermal conductivity detector (TCD) and flame ionization detector (FID).

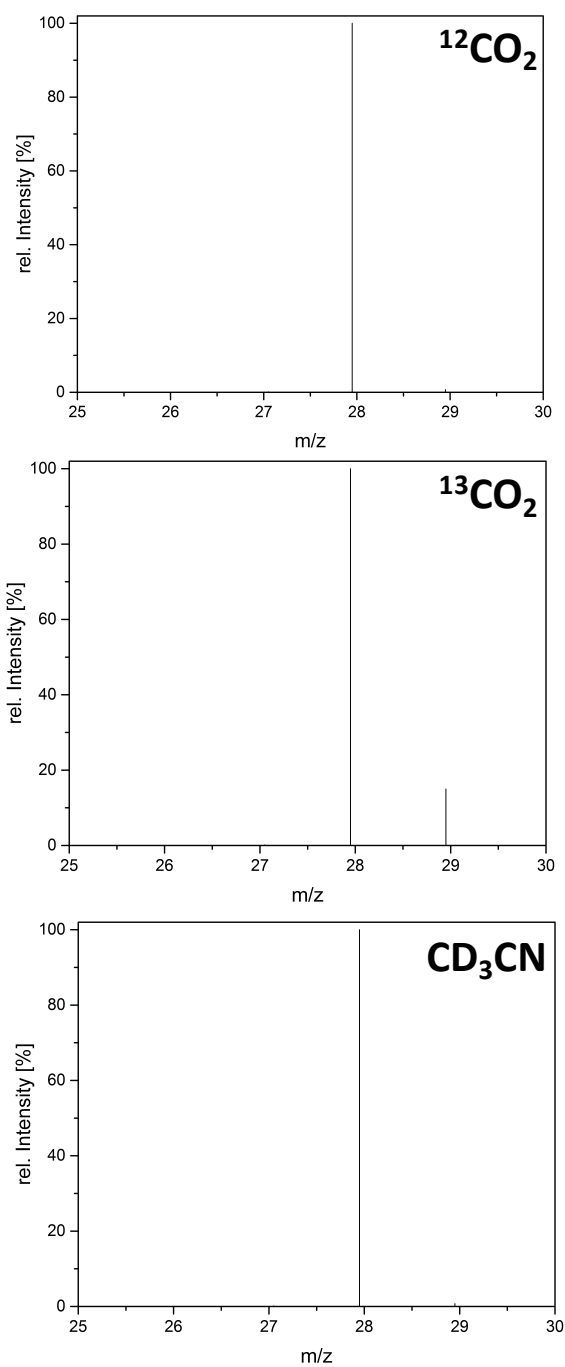


Figure S9. GC-MS control experiments using $^{12}\text{CO}_2$ (top), $^{13}\text{CO}_2$ (middle) gas and CD_3CN (bottom) showing the observed mass patterns of CO under the various reaction conditions. Note: N_2 and CO are not separated on a HP-PlotQ column. As such, the peak at m/z 28 displays both N_2 and CO.

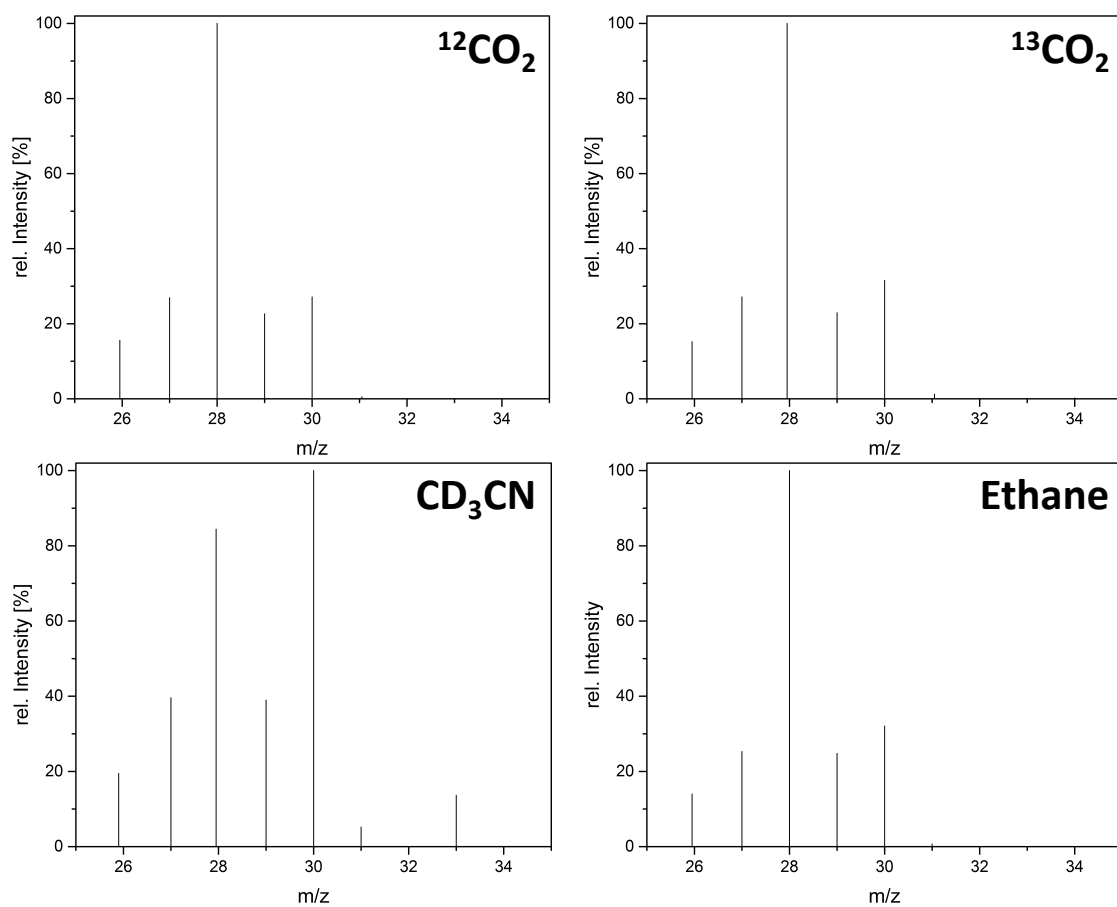


Figure S10. GC-MS control experiments using $^{12}\text{CO}_2$ (top, left), $^{13}\text{CO}_2$ (top, right) gas and CD_3CN (bottom, left) showing the observed mass patterns of ethane under the various reaction conditions. A comparative mass pattern for pure ethane is shown (bottom, right).

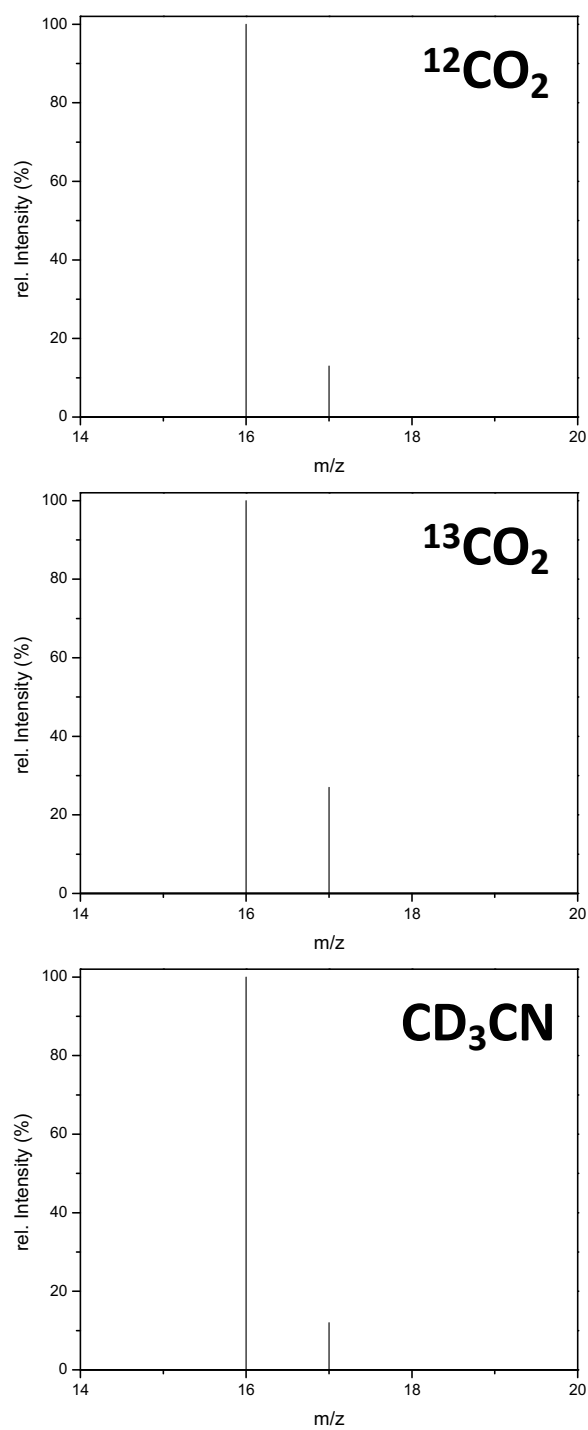


Figure S11. GC-MS control experiments using $^{12}\text{CO}_2$ (top), $^{13}\text{CO}_2$ (middle) gas and CD_3CN (bottom) showing the observed mass patterns of methane under the various reaction conditions.

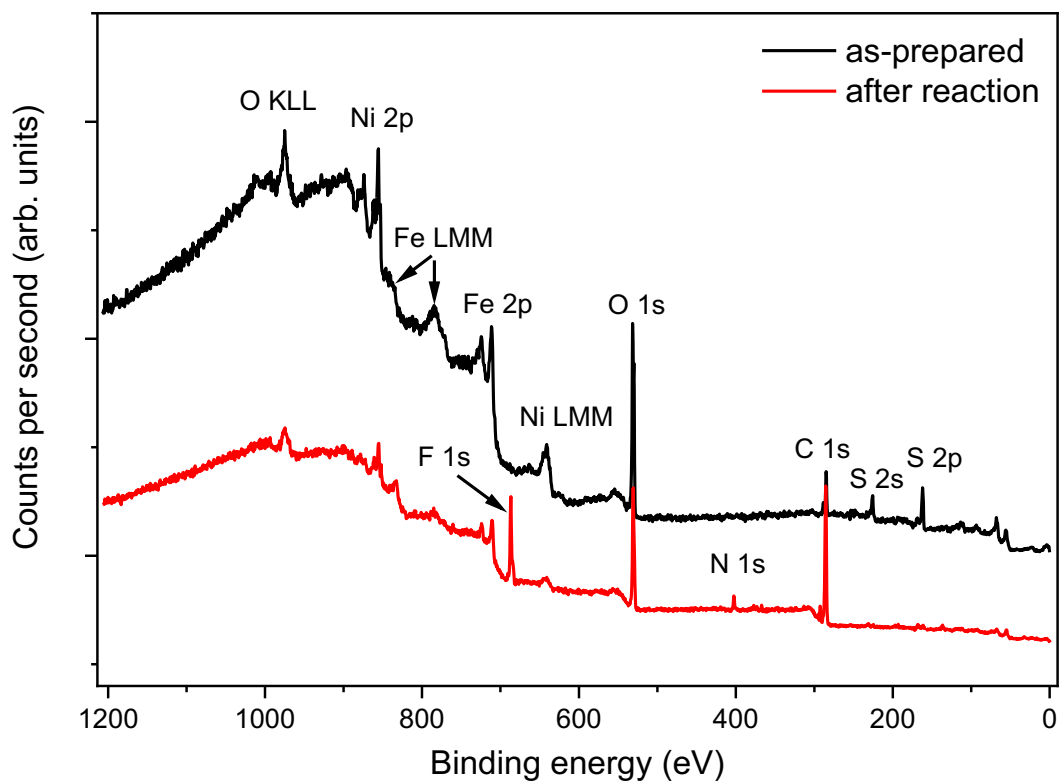


Figure S12. Survey XPS spectrum of the pentlandite sample before and after reaction in acetonitrile with 0.1 M TBAPF₆. The main photoemission and Auger are lines indicated.

Table S6. Distribution of disulfide species detected by XPS. FeS and NiS fractions of the overall observed Fe and Ni species are reported along with their ratio.

Sample	%FeS of total Fe	%NiS of total Ni	Fe : Ni observed	Fe : Ni expected
As-prepared	18	23	0.7	1
After CO2RR	16	19	0.8	1

References:

- [1] K. Junge Puring, S. Piontek, M. Smialkowski, J. Burfeind, S. Kaluza, C. Doetsch, U.-P. Apfel, *J. Vis. Exp. JoVE* **2017**, DOI 10.3791/56087.
- [2] C. S. Chen, A. D. Handoko, J. H. Wan, L. Ma, D. Ren, B. S. Yeo, *Catal. Sci. Technol.* **2015**, *5*, 161–168.
- [3] D. Gao, I. Zegkinoglou, N. J. Divins, F. Scholten, I. Sinev, P. Grosse, B. Roldan Cuenya, *ACS Nano* **2017**, *11*, 4825–4831.
- [4] D. Gao, F. Scholten, B. Roldan Cuenya, *ACS Catal.* **2017**, *7*, 5112–5120.
- [5] A. D. Handoko, C. W. Ong, Y. Huang, Z. G. Lee, L. Lin, G. B. Panetti, B. S. Yeo, *J. Phys. Chem. C* **2016**, *120*, 20058–20067.
- [6] S. Lee, D. Kim, J. Lee, *Angew. Chem. Int. Ed.* **2015**, *54*, 14701–14705.
- [7] A. Dutta, M. Rahaman, N. C. Luedi, M. Mohos, P. Broekmann, *ACS Catal.* **2016**, *6*, 3804–3814.
- [8] H. Yano, T. Tanaka, M. Nakayama, K. Ogura, *J. Electroanal. Chem.* **2004**, *565*, 287–293.
- [9] Y. Lum, B. Yue, P. Lobaccaro, A. T. Bell, J. W. Ager, *J. Phys. Chem. C* **2017**, *121*, 14191–14203.
- [10] F. Zhou, S. Liu, B. Yang, P. Wang, A. S. Alshammari, Y. Deng, *Electrochem. Commun.* **2014**, *46*, 103–106.
- [11] Y. Hori, H. Wakebe, T. Tsukamoto, O. Koga, *Electrochimica Acta* **1994**, *39*, 1833–1839.
- [12] K. Hara, A. Kudo, T. Sakata, *J. Electroanal. Chem.* **1995**, *391*, 141–147.
- [13] S. Ikeda, T. Takagi, K. Ito, *Bull. Chem. Soc. Jpn.* **1987**, *60*, 2517–2522.
- [14] J. L. DiMeglio, J. Rosenthal, *J. Am. Chem. Soc.* **2013**, *135*, 8798–8801.
- [15] A. Atifi, D. W. Boyce, J. L. DiMeglio, J. Rosenthal, *ACS Catal.* **2018**, *8*, 2857–2863.
- [16] E. Li, F. Yang, Z. Wu, Y. Wang, M. Ruan, P. Song, W. Xing, W. Xu, *Small* **2018**, *14*, 1702827.
- [17] C. Yan, H. Li, Y. Ye, H. Wu, F. Cai, R. Si, J. Xiao, S. Miao, S. Xie, F. Yang, et al., *Energy Environ. Sci.* **2018**, DOI 10.1039/C8EE00133B.
- [18] J. Zhang, T. Wang, P. Liu, Z. Liao, S. Liu, X. Zhuang, M. Chen, E. Zschech, X. Feng, *Nat. Commun.* **2017**, *8*, 15437.
- [19] D. A. Torelli, S. A. Francis, J. C. Crompton, A. Javier, J. R. Thompson, B. S. Brunshwig, M. P. Soriaga, N. S. Lewis, *ACS Catal.* **2016**, *6*, 2100–2104.
- [20] M. Asadi, B. Kumar, A. Behranginia, B. A. Rosen, A. Baskin, N. Reppin, D. Pisasale, P. Phillips, W. Zhu, R. Haasch, et al., *Nat. Commun.* **2014**, *5*, DOI 10.1038/ncomms5470.
- [21] M. Asadi, K. Kim, C. Liu, A. V. Addepalli, P. Abbasi, P. Yasaei, P. Phillips, A. Behranginia, J. M. Cerrato, R. Haasch, et al., *Science* **2016**, *353*, 467–470.
- [22] S. K. Kim, Y.-J. Zhang, H. Bergstrom, R. Michalsky, A. Peterson, *ACS Catal.* **2016**, *6*, 2003–2013.
- [23] D. L. T. Nguyen, M. S. Jee, D. H. Won, H. Jung, H.-S. Oh, B. K. Min, Y. J. Hwang, *ACS Sustain. Chem. Eng.* **2017**, *5*, 11377–11386.
- [24] J. J. Carroll, J. D. Slupsky, A. E. Mather, *J. Phys. Chem. Ref. Data* **1991**, *20*, 1201–1209.
- [25] P. G. T. Fogg, *Carbon Dioxide in Non-Aqueous Solvents at Pressures Less Than 200 KPa*, Pergamon Press, **1992**.
- [26] Y. Tomita, S. Teruya, O. Koga, Y. Hori, *J. Electrochem. Soc.* **2000**, *147*, 4164.
- [27] L. Hua, *Phys. Chem. Liq.* **2009**, *47*, 296–301.
- [28] P. D. Mantor, O. Abib, K. Y. Song, R. Kobayashi, *J. Chem. Eng. Data* **1982**, *27*, 243–245.
- [29] N. Elgrishi, K. J. Rountree, B. D. McCarthy, E. S. Rountree, T. T. Eisenhart, J. L. Dempsey, *J. Chem. Educ.* **2018**, *95*, 197.